Zhang and Sun
Journal of Engineering and Applied Science (2024) 71:125
https://doi.org/10.1186/s44147-024-00456-0

Journal of Engineering and Applied Science

RESEARCH Open Access

The analytical model of crimping springback for large-diameter longitudinal welded pipe

Ji Zhang[1] and Kai Sun[1*]

*Correspondence:
sunkai@dlut.edu.cn

[1] State Key Laboratory of Structural Analysis, Optimization and CAE Software for Industrial Equipment, Dalian University of Technology, Dalian, China

Abstract

The crimping technique is widely used in the manufacturing process of large-diameter longitudinal welded pipe. In the bending process, the springback is the critical problem affecting the shape, which is the key index of forming quality. So, crimping faces more challenges in accurate springback prediction for difficult-to-form metals such as pipeline steels and non-circular nature of the punch. This paper has established an analytical model of crimping springback for the longitudinal welded pipe. Firstly, the crimping process mathematical model which considered the impact of elastic modulus attenuation on springback calculation during plastic deformation is established, and the cross-section bending moment is calculated based on Hill's bending theory. Secondly, a semi-analytical and semi-numerical method for calculating the crimping shape is presented. Finally, the comparison of the crimping shape of the real product shows that the calculation accuracy and efficiency of this method can meet the requirements of engineering applications. The relative error of the springback angle calculated by the analytical model is −5.84%, and the absolute error is 0.3°. This method can accurately predict the springback of longitudinal welded pipe after crimping and provide a reference for crimping process optimization.

Keywords: Longitudinal welded pipe, Crimping, Springback, Analytical model

Introduction

The crimping process is used in the J shape-C shape-O shape (JCO) forming method of sheets for large-diameter longitudinally welded pipes. Before JCO forming, the prevention of quality defects, such as pouting and peach-shaped mouth in the finished pipe fittings, involves crimping the edge of the sheet first followed by JCO forming. Then, the bent sheet is sent into the JCO forming machine to bend half of the sheet into a "J" shape through multiple three-point free bending under a step-by-step process. The other half of the sheet is fed into a forming machine through a feeding mechanism, and the sheet is gradually bent into a "C" shape in a similar manner. The left and right sides, which present symmetrical geometric shapes, are finally bent to form an open "O" shape. The crimping process uses a crimping mold to press the edges of the steel plate on both sides. The edges are bent to a certain curvature to make sure it is close to or reaching the nominal curvature of the pipe. The technique ensures the geometric shape and dimensional

accuracy of the welded area of the final product. This process can effectively prevent weld distortion and cracking during expansion [1].

The crimping is a very complicated procedure since it is usually influenced by many factors. It is difficult to design technical parameters and control the forming quality. Early engineering technicians used classical bending theory to analyze the crimping process [2]. Shabalov et al. [3] described the entire process of crimping technique and summarized the reasonable range of various technical parameters. Fan et al. [4, 5] used plastic mechanics to analyze the mechanical properties of the crimping process and derived the main design formulas for crimping technical parameters and relevant formulas for crimping deformation using different ideal material models.

The classic engineering bending theory used in analyzing the crimping process neglects the impact of radial stress on bending springback and also does not consider the internal movement of neutral layers. Aiming to solve this issue, Hill [6] proposed a precision bending theory, which only applies the exact analysis method of the ideal rigid plastic bending but recommends the use of accurate analysis methods for bending. Based on this, many scholars introduced various hardening laws. Johnson and Yu [7] proposed springback formulae to describe linear and non-linear material work hardening in beams and plates. Queener and DeAngelis [8] used power law stress-strain relations to represent the hardening phenomenon of materials. Proksa [9] introduced the model of linear hardening material for springback calculations. Morestin et al. [10] proposed a theoretical analytical model to predict the springback of sheet metal based on the isotropic Von Mises yield criterion, the Lemaitre nonlinear dynamic strengthening criterion, and the incremental theory. This model has been successfully applied.

High-strength steels such as pipeline steel and magnesium-aluminum alloys exhibit elastic modulus attenuation during plastic deformation [11–13]. Research has found that the degree of unloading elastic modulus attenuation is closely related to plastic strain, heat treatment, chemical composition, and strain path [14–16]. To further improve the calculation accuracy of springback, the phenomenon of attenuation of elastic modulus during the forming process has attracted more and more attention. Whether classical engineering bending theory or Hill's accurate bending theory, the elastic modulus is often assumed to be constant in traditional springback analysis, which often results in significant discrepancies between the calculated values of springback and actual values. Lems [17] found that the elastic modulus of the material decreases gradually as the deformation degree increases, and compared with experimental studies and simulation results, it was found that numerical simulation results are generally less than the actual springback quantity of the metallic material. Morestin and Boivin [18] conducted uniaxial tensile experiments on different grades of steel and found that at a plastic strain of 5%, the elastic modulus dropped by 10%. The modulus of commonly used low-carbon steel, high-strength steel, and aluminum alloy decreases by 30%, 20%, and 10%, respectively, during the unloading process. Therefore, considering the changes in elastic modulus can significantly improve the accuracy of rebound calculation. Yoshida and Uemori [19] proposed a power law formula to describe the relationship between Young's modulus and cumulative plastic strain. By defining the chord modulus as the slope of the line between the stress point before unloading and the zero stress point after unloading, the nonlinearity of the unloading-reloading curve is ignored. This method is known as the chord modulus method. Yoshida and Amaishi [20]

proposed that stress factors are introduced on the string model to describe the nonlinear elastic deformation during unloading [21]. The effect of the elastic-plastic stress-strain transition on the rebound prediction is studied based on the Yoshida nonlinear elastic model. Qingdang et al. [22] use the Chaboche hardening model and the string modulus model to characterize the constitutive properties of the material. The analytical model has higher prediction accuracy and faster solution speed than the existing models.

With the development of computer technology, many researchers are using the finite element method to analyze the crimping process and its impact on the quality of welded pipes. Fan et al. [23–25] used the finite element software ABAQUS to analyze the crimping process, summarized the influence of mold parameters on the crimping shape, and verified that the involute mold surface is beneficial to improve the forming quality of welded pipes. Tang et al. [26] established a finite element analysis model for the three-dimensional crimping forming process and obtained the maximum load during the forming process. In addition, the commercial software ABAQUS has achieved excellent application effects in simulating the crimping forming process, obtaining geometric shape and stress-strain distribution of pipe blank after forming, and other aspects of forming quality [27–31].

In conclusion, the analysis of crimping forming is usually conducted using theoretical and numerical methods. The current crimping analytical theory adopts the engineering bending theory without considering the radial stress and the internal migration of the neutral layer, while ignoring the influence of the attenuation of the elastic modulus on the calculation of rebound. And the existence of numerous assumptions leads to low calculation accuracy. The introduction of precise bending theory has greatly increased the difficulty of solving the problem. On the other hand, using numerical calculation methods such as finite element analysis to calculate crimping forming springback is very time-consuming and seriously hinders its promotion and application in engineering. Therefore, this paper uses a chord model to calculate the springback of crimping forming, considering the attenuation of elastic modulus, using a combination of analytical and numerical methods. The purpose is to propose a calculation method for springback in crimping forming that combines both calculation accuracy and efficiency.

Methods

Crimping process

The sheet metal crimping process is shown in Fig. 1. The punch is usually fixed, and the cylinder drives the die to rise gradually. The sheet metal is gradually bent along the punch from point O to point A. When the sheet metal wraps around the punch, the crimping roll angle is α.

The surface curve of the crimping punch adopts the involute form, and the equation is:

$$\begin{cases} x(\varphi) = R_{\mathrm{p}}\cos\varphi + \varphi R_{\mathrm{p}}\sin\varphi \\ y(\varphi) = R_{\mathrm{p}}\sin\varphi + \varphi R_{\mathrm{p}}\cos\varphi \end{cases} \tag{1}$$

where R_{p} is the base circle radius, and ϕ is the base circle angle.

With the start point O as the origin, a coordinate system XOY is established. The involute curvature parameter of the crimping punch in the coordinate can be obtained as follows:

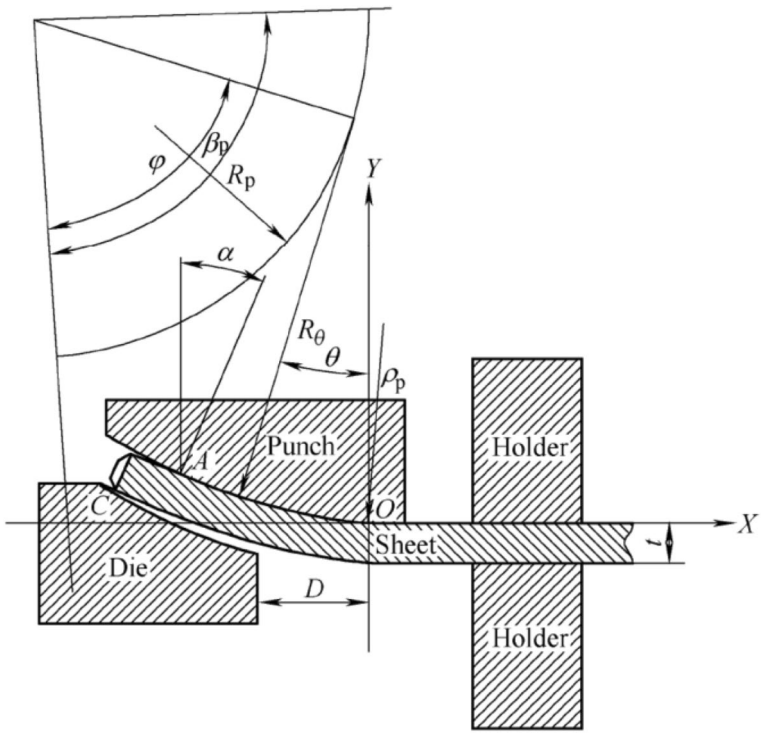

Fig. 1 Crimping and forming process [4]

$$\begin{cases} X(\varphi)=[x(\varphi)-x(\beta_P)]\cos\beta_P+[y(\varphi)-y(\beta_P)]\sin\beta_P \\ Y(\varphi)=-[x(\varphi)-x(\beta_P)]\sin\beta_P+[y(\varphi)-y(\beta_P)]\cos\beta_P \end{cases} \tag{2}$$

where β_P is the termination angle.

Then, the involute curvature of the crimping die is in contact with the sheet at point C, and its coordinates can be expressed as follows:

$$\begin{cases} X_C=X(\varphi_A)-L_z\cos\alpha-t\sin\alpha \\ Y_C=Y(\varphi_A)+L_z\sin\alpha-t\cos\alpha \end{cases} \tag{3}$$

where α is the crimping roll angle at point A, and L_z is the straight edge length, which can be calculated by the following equation:

$$L_z=B-\left[S+\frac{t}{2}\tan(\alpha)+P\right] \tag{4}$$

where t is the board material thickness, B is the crimping length, P is the slope width, and S is the curved edge arc length, which can be expressed as follows:

$$S=\frac{R_P}{2}\left(2\alpha\beta_P-\alpha^2\right) \tag{5}$$

According to the involute curvature property, the relationship between ϕ, θ, and the radius of punch R_θ can be expressed as follows:

$$\begin{cases} \theta = \beta_{\mathrm{p}} - \varphi \\ R_\theta = R_{\mathrm{p}} \cdot \varphi \end{cases} \tag{6}$$

As the crimping is unloaded, the sheet metal springback angle $\Delta\alpha$ is:

$$\Delta\alpha = \alpha - \alpha' \tag{7}$$

where α' is the roll angle after springback.

Calculation of sheet metal crimping moment

In order to simplify the calculation, the following assumptions are made according to the characteristics of the bending deformation of wide plate [12, 13]:

(1) Since the initial width of the sheet is much larger than the thickness of the sheet, the bending process is wide sheet bending, which means the strain along the width direction of the sheet can be ignored, that is $\varepsilon_{\mathrm{W}} = 0$.
(2) Assumption of a straight line.
(3) The volume remains constant during bending, that is $\varepsilon_{\mathrm{W}} + \varepsilon_\theta + \varepsilon_{\mathrm{r}} = 0$, where ε_θ is the tangential strain and ε_{r} is the normal strain.
(4) In the analysis process, the Bauschinger effect is not considered and the springback is only regarded as an elastic unloading process.

As the sheet metal is bent, the outer radius is $R_{\mathrm{o}} = R_{\mathrm{i}} + t/2$, and the inner radius is $R_{\mathrm{i}} = R_\theta$. According to Hill's bending theory, the neutral layer radius of stress is:

$$R_{\mathrm{n}} = \sqrt{R_{\mathrm{i}} R_{\mathrm{o}}} \tag{8}$$

The geometric center radius of the sheet section:

$$R_{\mathrm{m}} = \frac{R_{\mathrm{i}} + R_{\mathrm{o}}}{2} \tag{9}$$

According to the assumptions (1) and (3), we can get the equation of $\varepsilon_\theta = -\varepsilon_{\mathrm{r}}$. As to the characteristics of the bending deformation, the distribution of the tangential strain along the sheet thickness direction can be expressed as follows:

$$\varepsilon_\theta = \begin{cases} \frac{r - R_{\mathrm{n}}}{R_{\mathrm{n}}} & |r - R_{\mathrm{n}}| \le c \\ \mathrm{Ln}\frac{r}{R_{\mathrm{n}}} & |r - R_{\mathrm{n}}| \ge c \end{cases} \tag{10}$$

where c is the width of the elastic zone. The stress along the width direction ε_{W} can be obtained by the plane strain condition as follows:

$$\sigma_{\mathrm{W}} = \begin{cases} \frac{\sigma_\theta + \sigma_{\mathrm{r}}}{2} & r \ge R_{\mathrm{n}} \\ \frac{\sigma_\theta - \sigma_{\mathrm{r}}}{2} & r \le R_{\mathrm{n}} \end{cases} \tag{11}$$

where σ_θ is the tangential stress, σ_{r} is the normal stress. Bring the Eq. (11) into the equivalent effect force definition formula is available:

$$\overline{\sigma}=\begin{cases} -\frac{\sqrt{3}}{2}(\sigma_\theta+\sigma_\mathrm{r}) & r \geq R_\mathrm{n} \\ \frac{\sqrt{3}}{2}(\sigma_\theta-\sigma_\mathrm{r}) & r \leq R_\mathrm{n} \end{cases} \tag{12}$$

And according to the principle of equivalent plastic work:

$$\sum \sigma_{\mathrm{ij}}\varepsilon_{\mathrm{ij}}=\overline{\sigma}\,\overline{\varepsilon} \tag{13}$$

The equivalent strain can be obtained by inserting Eqs. (11–12) into (13):

$$\overline{\varepsilon}=\begin{cases} \frac{2}{\sqrt{3}}\varepsilon_\theta & R_\mathrm{n} \leq r \leq R_\mathrm{o} \\ -\frac{2}{\sqrt{3}}\varepsilon_\theta & R_\mathrm{I} \leq r \leq R_\mathrm{n} \end{cases} \tag{14}$$

According to the plastic condition $\overline{\sigma}=\sigma_\mathrm{s}$, the bending radius of the elastic limit when the sheet just enters the plastic state is:

$$\begin{cases} r_\mathrm{s}^{+}=\frac{\sqrt{3}(1+\mu)}{2E}\sigma_\mathrm{s}R_\mathrm{n}+R_\mathrm{n} & R_\mathrm{n}+c \leq r \leq R_\mathrm{o} \\ r_\mathrm{s}^{-}=R_\mathrm{n}-\frac{\sqrt{3}(1+\mu)}{2E}\sigma_\mathrm{s}R_\mathrm{n} & R_\mathrm{I} \leq r \leq R_\mathrm{n}-c \end{cases} \tag{15}$$

where r_s^{+} is the outer elastic radius, r_s^{-} is the inner elastic radius, μ is Poisson's ratio, and E is the elasticity modulus, and the elastoplastic boundary is:

$$c=|r_s-R_\mathrm{n}|=\frac{\sqrt{3}(1+\mu)}{2E}\sigma_\mathrm{s}R_\mathrm{n} \tag{16}$$

The constitutive relation of material in the plastic state is:

$$\overline{\sigma}=K\overline{\varepsilon}^{n} \tag{17}$$

where K is the intensity coefficient, and n is the hardening index. Inserting Eq. (10) to Eq. (17):

$$\overline{\sigma}=\begin{cases} K(\frac{2}{\sqrt{3}}\mathrm{Ln}\frac{r}{R_\mathrm{n}})^{n} & R_\mathrm{n}+c \leq r \leq R_\mathrm{o} \\ K(-\frac{2}{\sqrt{3}}\mathrm{Ln}\frac{\mathrm{r}}{R_\mathrm{n}})^{\mathrm{n}} & R_\mathrm{I} \leq r \leq R_\mathrm{n}-c \end{cases} \tag{18}$$

The stress balance equation in differential form can be expressed as follows:

$$r\frac{\mathrm{d}\sigma_\mathrm{r}}{\mathrm{d}r}=\frac{2}{\sqrt{3}}\overline{\sigma} \tag{19}$$

Inserting Eq. (18) to Eq. (19) and integrating. According to the boundary conditions, the normal stress in the plastic state can be expressed as follows:

$$\sigma_\mathrm{r}=\begin{cases} \frac{K}{n+1}\left[\left(\frac{2}{\sqrt{3}}\mathrm{Ln}(\frac{r}{R_\mathrm{n}}\right)^{n+1}-\left(\frac{2}{\sqrt{3}}\mathrm{Ln}(\frac{R_\mathrm{o}}{R_\mathrm{n}}\right)^{n+1}\right] & R_\mathrm{n}+c \leq r \leq R_\mathrm{o} \\ \frac{K}{n+1}\left[\left(\frac{2}{\sqrt{3}}\mathrm{Ln}(\frac{R_\mathrm{n}}{R_\mathrm{I}}\right)^{n+1}-\left(\frac{2}{\sqrt{3}}\mathrm{Ln}(\frac{R_\mathrm{n}}{r}\right)^{n+1}\right] & R_\mathrm{I} \leq r \leq R_\mathrm{n}-c \end{cases} \tag{20}$$

According to Eq. (19), the tangential stress can be expressed as follows:

$$\sigma_\theta = \begin{cases} r\frac{d\sigma_r}{dr} + \sigma_r & (r \geq R_n) \\ -r\frac{d\sigma_r}{dr} + \sigma_r & (r \leq R_n) \end{cases} \tag{21}$$

and the constitutive model of material in an elastic state is:

$$\begin{cases} \varepsilon_\theta = \frac{\sigma_\theta}{E'} - \mu'\frac{\sigma_r}{E'} \\ \varepsilon_r = \frac{\sigma_r}{E'} - \mu'\frac{\sigma_\theta}{E'} \end{cases} \tag{22}$$

where $E' = \frac{E_0}{1-\mu^2}$, $\mu' = \frac{\mu}{1-\mu}$. Further derivation can be obtained:

$$\sigma_\theta = \frac{E'\left[\varepsilon_\theta - \mu'\varepsilon_r\right]}{1 - \mu'^2} \tag{23}$$

The bending moment is related to the tangential stress in the cross-section, and the elastic bending moment can be expressed as:

$$\begin{cases} M_{eo} = \int_{R_n}^{r_s^+} \sigma_\theta (r - R_n) dr & \left(R_n \leq r \leq r_s^+\right) \\ M_{ei} = \int_{r_s^-}^{R_n} \sigma_\theta (R_n - r) dr & \left(r_s^- \leq r \leq R_n\right) \end{cases} \tag{24}$$

where M_{eo} is the outer elastic bending moment, and M_{ei} is the inner elastic bending moment. The plastic bending moment can be expressed as:

$$\begin{cases} M_{pi} = \int_{R_i}^{r_s^-} \sigma_\theta (R_n - r) dr \left(R_i \leq r \leq r_s^-\right) \\ M_{po} = \int_{r_s^+}^{R_o} \sigma_\theta (r - R_n) dr \left(r_s^+ \leq r \leq R_o\right) \end{cases} \tag{25}$$

where M_{pi} is the inner plastic bending moment, and M_{po} is the outer plastic bending moment. The bending moment of the cross-section can be expressed as:

$$M = M_{ei} + M_{eo} + M_{pi} + M_{po} \tag{26}$$

Calculation of springback

Through previous research, it was found that the elastic modulus decreases with increasing plastic deformation. Therefore, Yoshida and Uemori [19] proposed a widely used chord model to describe this experimental phenomenon:

$$E_{chord} = E_0 - (E_0 - E_a)[1 - \exp(-\xi p)] \tag{27}$$

where E_0 is the initial elastic modulus, E_a is the saturated elastic modulus, p is the plastic strain, and ξ is a coefficient related to materials.

$$p = \ln\left(\frac{r}{R_n}\right) - \frac{\sigma_\theta}{E_0} \tag{28}$$

The calculation of plastic strain p has been approximated in this paper:
The springback strain can be expressed as:

$$\Delta\varepsilon = \mathrm{Ln}\left(\frac{r_f}{R_{nf}}\right) - \mathrm{Ln}\left(\frac{r}{R_n}\right) \tag{29}$$

$$r_f = R_{nf} - R_n + r \tag{30}$$

where R_{nf} is the curvature radius after bending springback, and R_{n} is the curvature radius before bending springback. So, the springback strain can be rewritten as:

$$\Delta\varepsilon = \mathrm{Ln}\left(\frac{R_{nf} - R_n + r}{R_{nf}}\right)\left(\frac{R_n}{r}\right) \tag{31}$$

The springback stress can be expressed as:

$$\Delta\sigma = E_{Chord}\Delta\varepsilon \tag{32}$$

The springback moment can be expressed as:

$$M_{\mathrm{springback}} = 2\int_{R_{\mathrm{n}}}^{t/2}\Delta\sigma(r - R_{\mathrm{n}})\mathrm{d}r \ \ (R_{\mathrm{n}} \le r \le t/2) \tag{33}$$

According to the unloaded law, the change of curvature after bending springback is:

$$M = M_{\mathrm{springback}} \tag{34}$$

where R_{nf} is the curvature radius after bending springback, and R_{n} is the curvature radius before bending springback.

Discrete plate element model

Discrete thinking is introduced in the numerical model, which involves dividing the crimping sheet along its center line into several discrete plate elements. When the plate elements are small enough, the shear effect caused by the crimping deformation can be ignored. For each plate element, the bending theory mentioned in the "Methods" section can be used for the analysis. According to the characteristics of crimping deformation of sheet metal, the geometric information of the coordinate origin remains unchanged during the bending process. The crimping forming shape is fitted by the geometric information after springback of discrete plate elements.

In order to establish the numerical model of crimping springback for sheet metal, the following assumptions are made for discrete plate elements:

(1) Each discrete plate element satisfies the bending theory in the "Methods" section.
(2) During the bending process, the arc length of the neutral layer of the discrete plate element remains unchanged.
(3) Each discrete plate element is a circular arc.

Divide the crimping section into k microelements, and its step size is:

$$\Delta L = \frac{B - L_{\mathrm{z}}}{k} \tag{35}$$

When loaded, the arc length of the microelement is:

$$S_{\mathrm{i}} = \rho_{\mathrm{i}}\mathrm{d}\beta \ \ \mathrm{i} = 1, 2, 3 \ldots \mathrm{k} \tag{36}$$

where ρ_i is the radius of arc curvature which can be determined by the following equation:

$$\rho_i=\frac{R_{nf(i)}+R_{nf(i+1)}}{2} \tag{37}$$

The relationship of $S_i = \Delta L$=ds can be obtained by assumption (2) in the "Results and discussion" section, and $\varphi_0 = \beta_p$ can be obtained based on the characteristics of crimping deformation. According to the triangle relation in Fig. 1, the following equations can be obtained:

$$\begin{cases} \Delta x_i=ds \cdot \cos\left(\frac{1}{2}d\beta_i+\theta_i\right) \\ \Delta y_i=ds \cdot \sin\left(\frac{1}{2}d\beta_i+\theta_i\right) \end{cases} \tag{38}$$

where Δx_i and Δy_i is the increment of horizontal and vertical, respectively, and the coordinates of the next step can be obtained:

$$\begin{cases} x_{i+1}=x_i+\Delta x_i \\ y_{i+1}=y_i+\Delta y_i \end{cases} \tag{39}$$

The initial position of the coordinate system is:

$$\begin{cases} X_0=0 \\ Y_0=\frac{R_1-R_n}{2} \end{cases} \tag{40}$$

The θ_i is updated as follows:

$$\theta_{i+1}=\theta_i+d\beta_i \tag{41}$$

when $i=k$, the corresponding angle is the roll angle of point A after springback:

$$\alpha=\theta_n \tag{42}$$

Results and discussion

Model verification

The crimping process of $\Phi 1219 \times 22 \times 12{,}000$ mm large-diameter straight seam-welded pipe is taken as an example, a metal plate size of 3720 mm × 22 × 12,000 mm was used, and a #3 crimping mold was adopted. The crimping parameters are shown in Table 1.

In order to adapt to the operating conditions of oil and gas pipelines such as high pressure and large deformation, the material performance objectives of high strength, high toughness, and large plasticity are often achieved through two-phase or multiphase structures. Therefore, the dual phase structure of bainite (B) + ferrite (PF) pipeline steel has gradually become a new hot spot in the field of pipeline steel research. The experimental material

Table 1 Crimping parameters

R_p (mm)	β_P (°)	B (mm)	L_Z (mm)	t (mm)
303.2	88	190	22	22

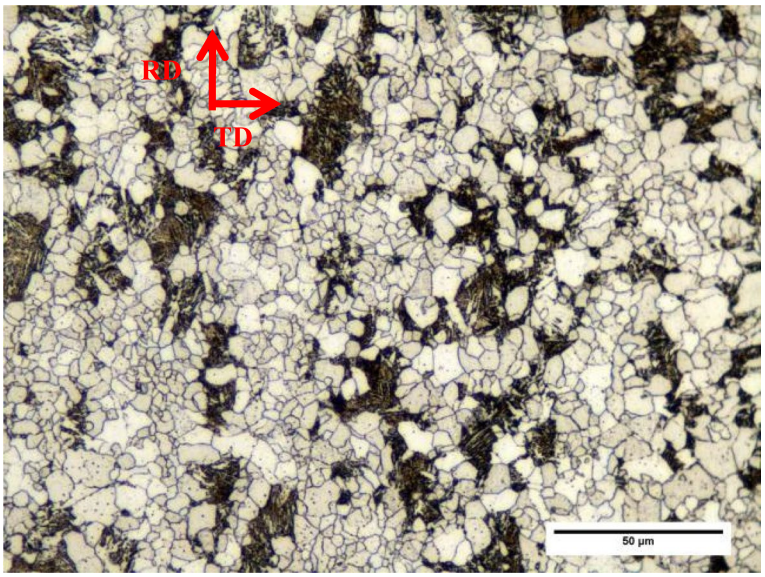

Fig. 2 Metallographic structure of X80 pipeline steel

Table 2 Material parameters

E (Gpa)	μ	σ_s (MPa)	K (MPa)	E_0 (Gpa)	ξ	E_a (Gpa)	n
197.135	0.3	590	918	197.135	− 76.78	157.795	0.077

used in this paper is X80 grade (B + PF) pipeline steel produced by Jiangsu Shagang Group Co., Ltd. Its main chemical composition (%, mass fraction) is C: 0.0931; Si: 0.25; Mn: 1.5, $P < 0.00005$; S: 0.0005; Cr: 0.136; Ti: 0.0138. The metallographic structure of X80 pipeline steel is shown in Fig. 2. The gray-white block is ferrite, and the core is scattered with black M-A island components. Except for the block ferrite, the other black parts are granular bainite and lath bainite. Movable dislocation in ferrite in pipeline steel with bainite and ferrite duplex structure can be easily started to obtain high-density dislocation. With the increase of the applied stress, the dislocation in ferrite slides to the bainite/ferrite interface and ferrite/ferrite interface and accumulates at the grain boundary, phase boundary, and precipitate. At the same time, there is a certain plastic strain incompatibility at the ferrite/bainite two-phase interface, so there is a large amount of dislocation accumulation and entanglement in the ferrite near the phase interface. The deformation characteristics of these materials are the main reasons for the nonlinear elastic behavior of high-strength pipeline steel.

The uniaxial tensile test of X80 grade (B + PF) pipeline steel is conducted by SANS static mechanical tensile test machine at room temperature, and the strain is measured by a 50-mm cutting edge extensor with an accuracy of microns and a strain rate of 0.001 s^{-1}. The tensile specimen shall be processed according to the national standard for tensile test of metal materials (GBT 228.1-2010). The five prestrains selected for unloading in the experiment were 1.5%, 3%, 4.5%, 6%, and 7.5%, and unloading was achieved by programming of a computer control system connected to the MTS810 experimental system. Table 2 can be obtained by processing the uniaxial tensile test data.

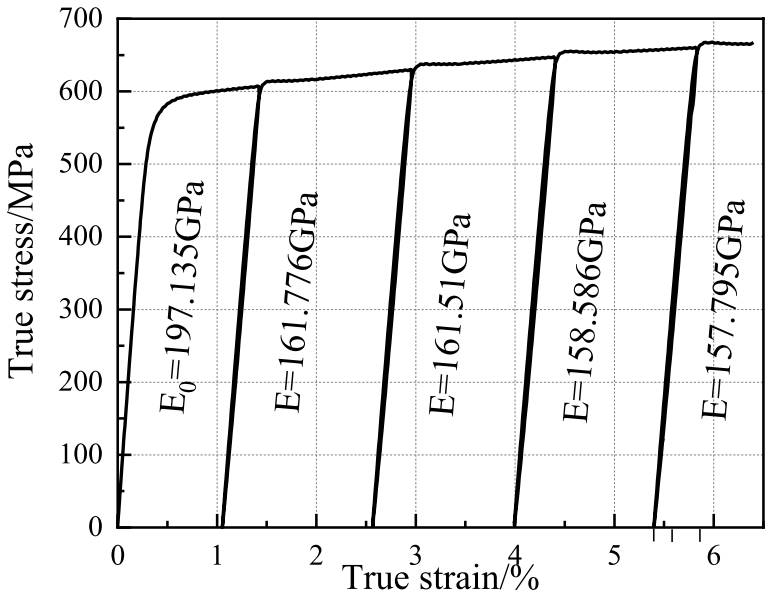

Fig. 3 Uniaxial cyclic loading and unloading experiment

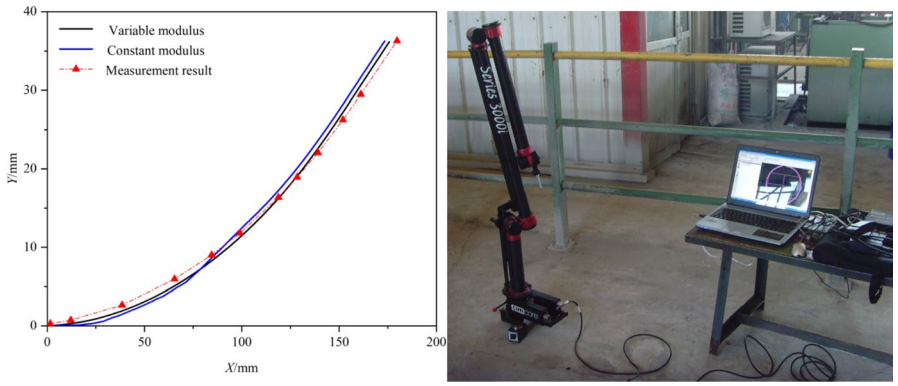

（a）Comparison of calculation and measurement （b）3D coordinate measuring equipment

Fig. 4 Experimental procedure of crimping measurement. **a** Comparison of calculation and measurement. **b** 3D coordinate measuring equipment

The stress-strain curve shown in Fig. 3 can be obtained by uniaxial cyclic loading and unloading experiment. It can be seen from the figure that the plastic deformation is large and the elastic modulus attenuation is large.

A 3D coordinate measuring equipment in Fig. 4b is used to get the coordinate information of the upper surface of sheet after crimping in the factory. The comparison of model calculation result and measurement is shown in Fig. 4a.

The comparison of model calculation and actual measurement results for the crimping roll angle is shown in Table 3. Taking the measured results as benchmark, the relative error of the springback angle calculated by the analytical model is −5.84%, and the absolute error is 0.3°. The errors are within the permissible range of engineering applications.

Table 3 Crimping roll angle

Parameters	Calculation result (°)	Measurement result (°)	Relative error (%)
Roll angle α	23.01	22.43	2.59
Angle after springback α'	18.16	17.29	5.03
Springback angle $\Delta\alpha$	4.84	5.14	−5.84

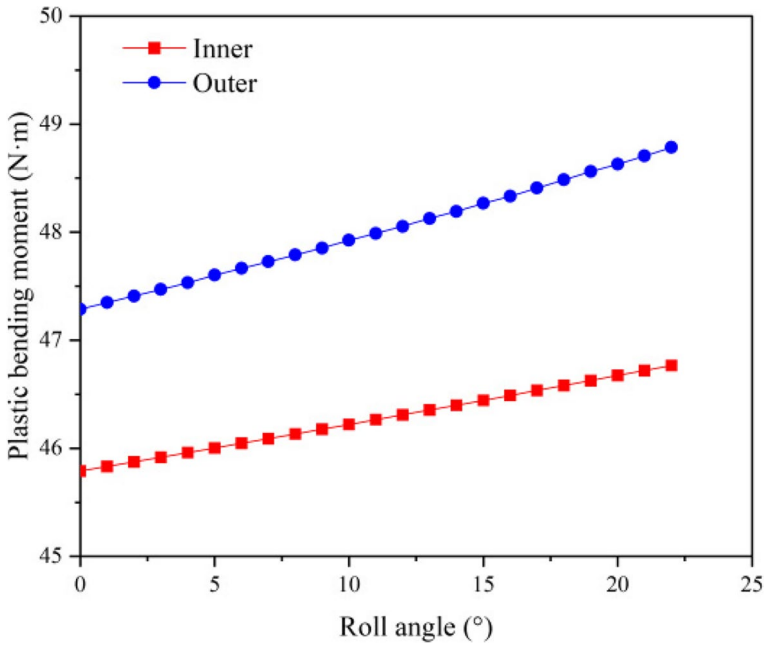

Fig. 5 Relationship of plastic bending moment and crimping roll angle

The main reasons for the errors in the calculation results are analyzed as follows:

(1) There are still many assumptions in the analytical model that deviate from the actual situation.
(2) Due to the wear of crimping die in the long-term production, there is a certain error with the calculated model.
(3) The constitutive model used in the analytical model calculation has some errors with the real material.

Analysis of deformation process

In the range of crimping roll angle 0 ~ 25°, the relationship between the cross-sectional bending moment and roll angle is obtained by the analytical model in the "Results and discussion" section. The plastic bending moment increases with the crimping roll angle, as shown in Fig. 5. The elastic bending moment decreases with the crimping roll angle, as shown in Fig. 6. The outer bending moment is greater than the inner bending moment. This is because the analytical model takes the inward movement of the neutral layer into

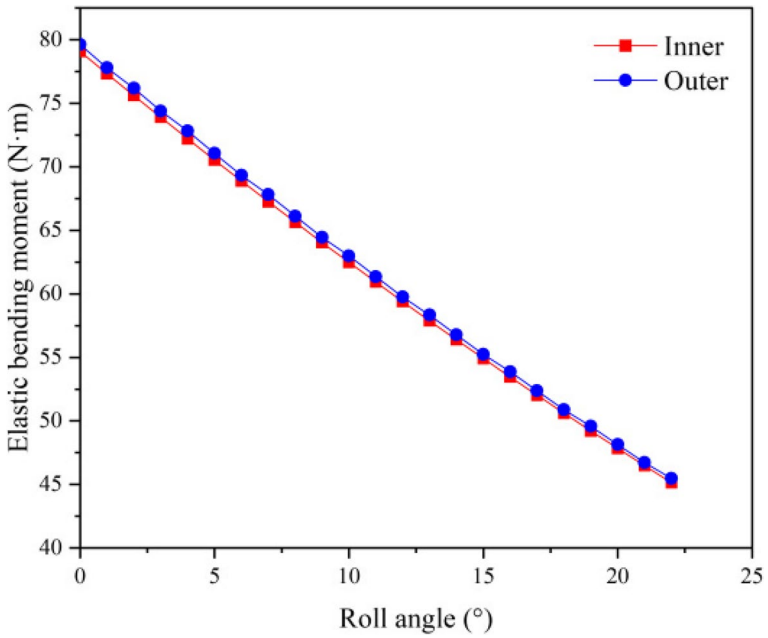

Fig. 6 Relationship of elastic bending moment and crimping roll angle

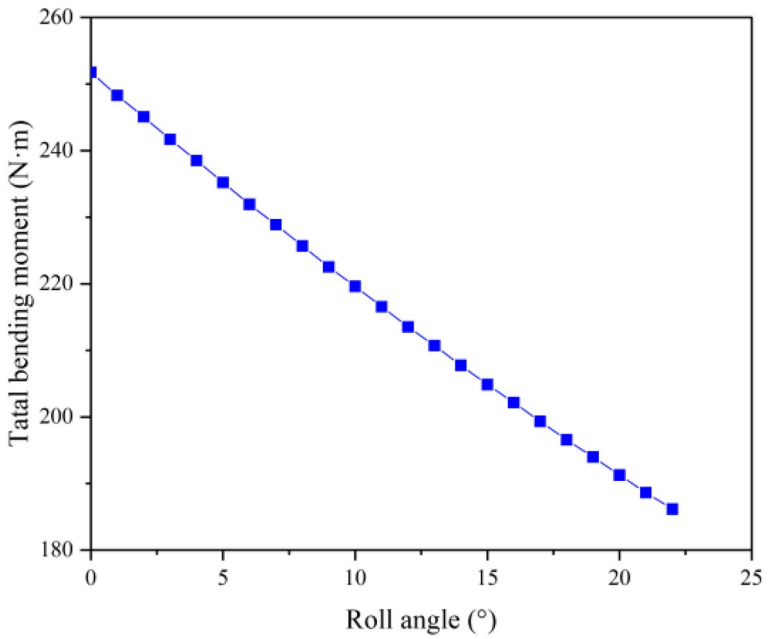

Fig. 7 Relationship of total bending moment and crimping roll angle

account, which means the farther away from the neutral layer, the greater value of the outer shear stress, while the inner shear stress is opposite.

In addition, the calculation results show that the total bending moment of the cross-section decreases as the crimping roll angle increases, as shown in Fig. 7. This is because the curvature radius decreases as the crimping roll angle increases, as shown in Fig. 8. Figure 9 shows the distribution of tangential stress and radial stress

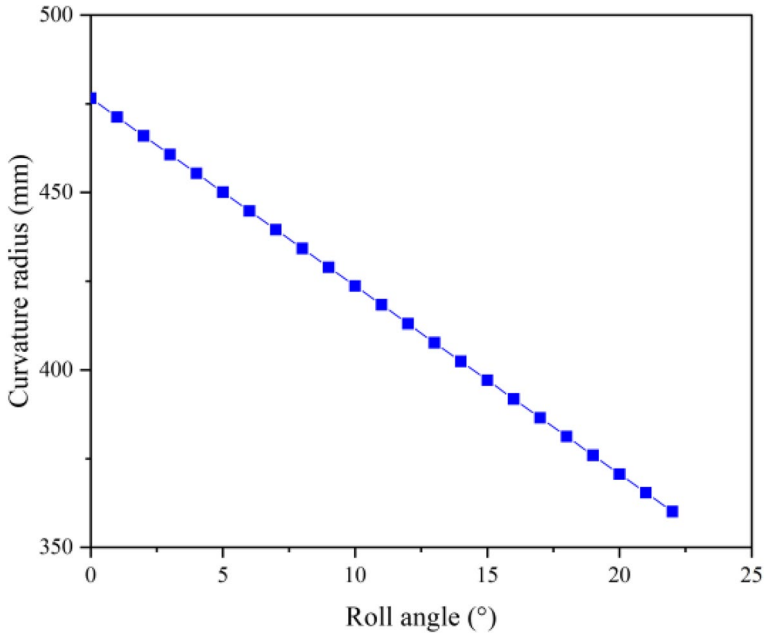

Fig. 8 Relationship of curvature radius and crimping roll angle

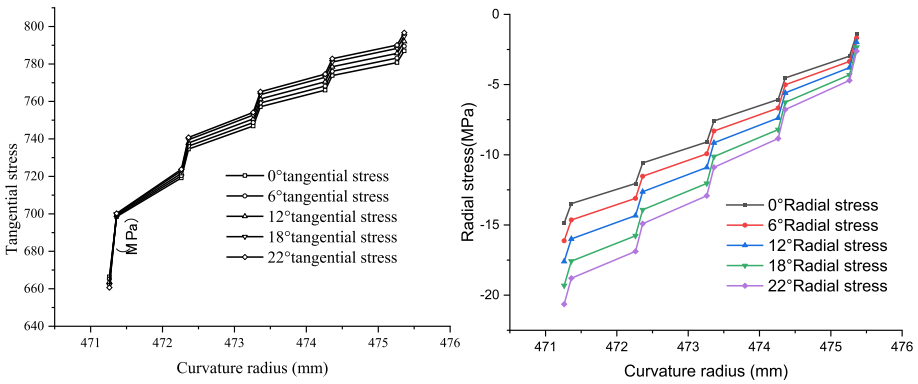

（a ） distribution of tangent stress （b） distribution of radial stress

Fig. 9 Distribution of tangent stress and radial stress bu'tong. **a** Distribution of tangent stress. **b** Distribution of radial stress

in the thickness direction of different crimping angles in the plastic zone. It can be seen from Fig. 10 that the tangential stress of different crimping angles increases as they approach the surface, and the tangential stress decreases as they approach the surface. For the same crimping angle, the tangential stress increases with the increase of curvature radius, while the radial stress increases with the increase of curvature radius.

As shown in Fig. 10, the larger the crimping angle, the greater the inward movement of the neutral layer. The smaller the elastic area.

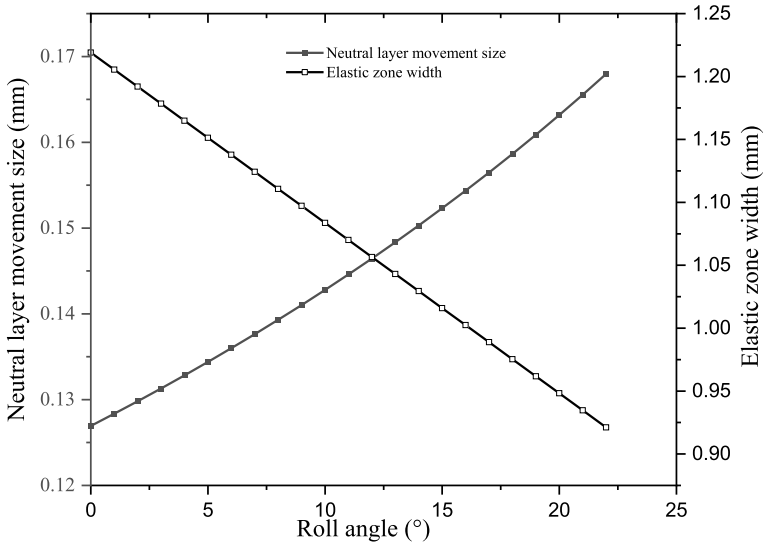

Fig. 10 Neutral layer movement and elastic zone width

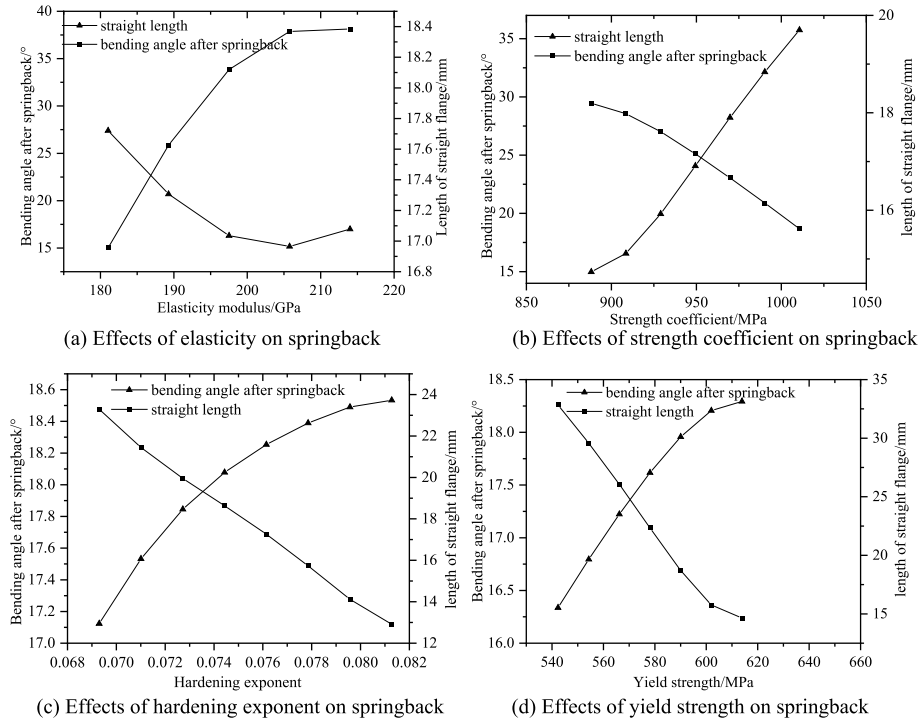

(a) Effects of elasticity on springback

(b) Effects of strength coefficient on springback

(c) Effects of hardening exponent on springback

(d) Effects of yield strength on springback

Fig. 11 Effects of material parameters on bending angle after springback of crimping and straight length. **a** Effects of elasticity on springback. **b** Effects of strength coefficient on springback. **c** Effects of hardening exponent on springback. **d** Effects of yield strength on springback

Effects of material parameters on springback of crimping

The quality of crimping depends on the bending angle after springback. However, material parameters can affect the bending angle after springback, so it is necessary to discuss the effects of material parameters on the bending angle and straight length.

In Fig. 11, the bending angle after springback monotonically increases with the increase of elastic modulus, yield strength, and hardening exponent. The bending angle after springback monotonically decreases with the increase of strength coefficient. The straight length monotonically decreases with the increase of strength coefficient, yield strength, and hardening exponent. From the figure, it can be seen that the elastic modulus and strength coefficient have a significant impact on the bending angle after springback, while the hardening index and yield strength have a relatively small impact on it. On the contrary, the elastic modulus has little effect on the length of the straight edge.

Conclusions

The precise control of sheet crimping is a critical technique in the forming of large-diameter longitudinal welded steel pipes, and it is very important to accurately calculate the amount of springback of crimping roll angle. Based on Hill's bending theory, a semi-analytical and semi-numerical calculation model is proposed by introducing a discrete numerical calculation method. By comparing the calculation model with the actual results of sheet crimping, it is found that the calculation accuracy of this model is relatively high, and the proposed model can meet the requirements for the crimping forming springback angle calculation in engineering.

Abbreviations

B Bainite
PF Ferrite

Acknowledgements
Not applicable.

Authors' contributions
ZJ: conception, theoretical derivation, experimental verification, result analysis, and writing of the paper.

Funding
The authors did not receive specific funding.

Availability of data and materials
All data generated or analyzed during this study are included in this published article.

Declarations

Competing interests
The authors declare that they have no competing interests.

Received: 4 September 2023 Accepted: 16 May 2024
Published online: 01 June 2024

References

1. Liu Q, Wan X (2019) Design of curvature radius of finishing roll for crimp JCO formed welded pipe. Open Access Libr J 6:e5759
2. Samusev SV, Zhigulev GP, Fadeev VA (2017) Edge geometry of pipe blanks produced by JCOE flexure. Steel Transl 47(5):296–298
3. Shabalov IP, Solovev DM, Filippov GA, Livanova OV (2015) Mechanical properties of a pipe workpiece at the stages of JCOE pipe forming. Russ Metall Met 2015(4):309–316
4. Fan L, Gao Y, Gao Y et al (2012) Quality control on crimping of large diameter welding pipe. Chin J Mech Eng 25(6):1264–1273
5. Fan LF, Liang P, Wang G, Gao Y, Zhang B (2019) Precision forming technology for crimping of large straight welded pipes. Adv Mater Sci Eng 2019:1–9
6. Hill R. The mathematical theory of plasticity. Oxford University Press; 1950.
7. Johnson W, Yu T (1981) Springback after the biaxial elastic-plastic pure bending of rectangular plate-I. Int J Mech Sci 23(10):619–630

8. Queener CA, DeAngelis RJ (1968) Elastic springback and residual stresses in sheet metal formed by bending. ASM Trans 61:757–768
9. Proksa F. Zur Theoriedes Plastischen Blechbiegens. Uni-hannover: Dissertation; 1958.
10. Morestin F, Boivin M, Silva C (1996) Elastic-plastic formulation using a kinematic hardening model for springback analysis in sheet metal forming. J Mater Process Technol 56(1–4):619–630
11. Wagoner RH, Lim H, Lee MG (2013) Advanced issues in springback. Int J Plast 45:3–20
12. Chen Z, Gandhi U, Lee J et al (2016) Variation and consistency of Young's modulus in steel. J Mater Process Technol 227:227–243
13. Ouyang F, Lu S, Fang J et al (2019) Effect of plastic strain on instantaneous elastic modulus of 21-6-9 high strength stainless steel tube. J Plast Eng 26(3):203–211
14. Zhang J, Li S, Ma W et al (2018) Influence of prestretching on bending springback of different high strength steels used in automobile. Forg Stamp Technol 43(12):26–30
15. Fei D, Hodgson P (2006) Experimental and numerical studies of springback in air V-bending process for cold rolled TRIP steels. Nucl Eng Des 236(18):1847–1851
16. Pavlina EJ, Levy BS, Van Tyne CJ (2008) The unloading modulus of ADKQ steel after uniaxial and near plane-strain plastic deformation. Int J Mod Phys B 22(31–32):6070–6075
17. Lems W (1963) The Change of Young's modulus after deformation at low temperature and its recovery. University of Delft, Delft
18. Morestin F, Boivin M (1996) On the necessity of taking into account the variation in the Young's modulus with plastic strain in elasti-plastic software. Nucl Eng Des 162:107–117
19. Yoshida F, Uemori T (2003) A model of large-strain cyclic plasticity and its application to springback simulation. Int J Mech Sci 45:1687–1702
20. Yoshida F, Amaishi T (2020) Model for description of nonlinear unloading-reloading stress-strain response with special reference to plastic-strain dependent chord modulus. Int J Plast 130:102708–102708
21. Yoshida F. Description of elastic-plastic stress-strain transition in cyclic plasticity and its effect on springback prediction. Int J Mater Form. 2022;015(2):12.
22. Qingdang M, Ruixue Z, Yu Z et al (2022) Analysis of springback for multiple bending considering nonlinear unloading-reloading behavior, stress inheritance and Bauschinger effect. J Mater Process Technol 307:117657
23. Fan LF, Gao Y, Yun JB et al (2015) Multi-objective optimization of crimping of large-diameter welding pipe. J Cent South Univ 22(7):2540–2548
24. Fan LF, Gao Y, Yun JB et al (2014) Deformation characteristic analysis on crimping of large diameter welding pipe. Adv Mater Res 986–987:1011–1014
25. Yan JX, Yun JB, Fan LF (2014) Effects of mould on crimping of large diameter welding pipe. Appl Mech Mater 623:129–132
26. Tang D, Peng Y, Li D et al. Numerical study on the X80 UOE pipe forming process. J Mater Process Tech. 2015;215:264–77.
27. Herynk MD, Kyriakides S, Onoufriou A et al (2007) Effects of the UOE/UOC pipe manufacturing processes on pipe collapse pressure. Int J Mech Sci 49(5):533–553
28. Gianfranco P, Luigi T (2005) Effect of forming and calibration operations on the final shape of large diameter welded tubes. J Mater Process Technol 164:1089–1098
29. Jian-xing Yu, Han M-X, Yang Yu, Duan J-H, Chen H-C (2021) The research on pipe structural behavior of 3D UOE manufacturing process. Thin-Walled Struct 158(1):8123–8231
30. Yu K, Choi H, Ha J et al (2023) Bauschinger effect calibration by the different types of loading/reverse loading tests for springback prediction in sheet metal forming. IntJ Mater Form 16:16
31. Li H, Chen S-F, Zhang S-H, Xu Y, Song H-W (2022) Deformation characteristics, formability and springback control of titanium alloy sheet at room temperature. A review. Materials 15:5586